Appl. Phys. A 81, 93–101 (2005)
DOI: 10.1007/s00339-004-3033-z

**Applied Physics A**
**Materials Science & Processing**

C. HUBER
T. KLAMROTH✉

# Simulation of two-photon-photoelectron spectra at a jellium-vacuum interface

Universität Potsdam, Institut für Chemie, Theoretische Chemie, Karl-Liebknecht-Straße 24–25, 14476 Golm, Germany

**Received: 26 May 2004/Accepted: 19 August 2004**
**Published online: 7 October 2004 •** 

**ABSTRACT** In this paper we report on time dependent configuration interaction singles (TD-CIS) calculations aimed at simulating two-photon-photoelectron emission (2PPE) spectra of metal films, the latter treated within a one-dimensional jellium model. The method is based on a many-electron approach in which electron-electron-scattering is approximately accounted for and no artificial lifetimes have to be assumed for excited electrons. This contrasts with one-electron models where lifetimes and "dissipation" have to be introduced. The driving force for the photoelectron ejection in 2PPE experiments is the electric field of two laser pulses that are generally separated by a delay time, $\Delta t$. To compute energy- and time-resolved 2PPE signals $P(E, \Delta t)$, a new scheme based on the time-energy method is proposed to analyze electronic wave packets in asymptotic regions of the potential.

**PACS** 78.20.Bh; 79.60.Bm

## 1 Introduction

Many physical and chemical properties/transformations at solid surfaces are due to electronic excitations. A good example is the manipulation of atomic or molecular species adsorbed at metal substrates, by UV/visible lasers. These create, in a first step, "hot electrons" within the metal which, for example, in a second step, transfer energy to a bond to be broken [1]. A second example is two-photon-photoemission (2PPE) spectroscopy of bare and adsorbate covered metal surfaces. This powerful spectroscopical technique, which comes in energy-, time- (TR-2PPE, time-resolved 2PPE), and angle-resolved (AR-2PPE) flavors, has been successfully used to measure the energetic position, and, more importantly, the energy and phase relaxation times of (excited) electronic bulk states [2], image potential states [3, 4], quantum well states [5], or adsorbate excited states [6]. The lifetimes of the excited states after laser excitation are often as short as fs ($10^{-15}$ s), and are largely determined by inelastic electron-electron scattering [7]. On a longer timescale (typically ps, ($10^{-12}$ s)), electron-phonon coupling sets in.

✉ Fax: +49-331-977-5058, E-mail: klamroth@rz.uni-potsdam.de

The basic steps of a TR-2PPE experiment are as follows: Electrons are excited from below the Fermi level, $E_F$, by a first laser pulse, causing a non-equilibrium energy distribution. A second laser pulse lifts the excited electrons from an "active energy space" into the vacuum region where their kinetic energy can be probed. By varying the delay time between the lasers, $\Delta t$, the actual population in the intermediate states can be determined. Hence the method is well suited to not only determine the location and dispersion of electronic states, but also their lifetime.

Most theoretical treatments of excited electron dynamics at metal interfaces make use of a one-electron picture [8–11]. In these models single electrons are moving in an effective one-particle potential, possibly coupled to an external laser field [10]. This is appropriate, as long as the selected electron can in some sense be considered independent and separated from the others. This is the case for electrons in image potential states, or electrons that decay from a negatively charged adsorbate (negative ion resonance) into the metallic substrate [8]. The separation of electrons from others is, however, by no means obvious for bulk electrons. Further, when modeling 2PPE spectra of decaying states, lifetimes due to electron-electron scattering have to be assumed for the intermediate states in one-particle theories. Hence, the dynamics of electrons must then be treated by a density matrix rather than a wavepacket approach [10]. However, it should be mentioned that those lifetimes can be calculated in very good agreement with experimental 2PPE results within in the framework of many-body perturbation theory, e.g., the GW approximation for the electronic self-energy (see [12, 13] and references therein).

As an alternative, one may use a many-electron description from the outset. Here electron-electron scattering is automatically accounted for and therefore no lifetimes need to be introduced. On the other hand, since we are ultimately interested in explicitly time dependent dynamics of electrons in nano-structured materials such as metal films or clusters, it is clear that a fully ab initio description is presently out of reach and other approximations need to be made.

One method to solve time dependent, many-electron Schrödinger equations in an approximate fashion is (explicitly) time dependent density functional theory (TD-DFT), another one its Hartree–Fock analog, TD-HF. Especially the TD-DFT method is widely used for describing laser-driven

processes in small metal clusters [14]. However, the quality of TD-DFT results depend very much on the quality of the exchange-correlation functional used and little is known about suitable functionals for one dimensional models, which we want to use here. In [15, 16], therefore, as an alternative an explicitly time dependent variant of the configuration interaction singles (TD-CIS) method [17] has been proposed. In this method, while still simple, the electronic wavefunction is expanded as a sum of HF and singly-excited Slater determinants, and correlation energy (for excited states) is explicitly included. The method is suited for short-time dynamics dominated by one-electron excitations.

A possible drawback of this method is that the ground state is identical to the HF ground state Slater determinant, which includes the well known problems in the treatment of metallic systems, most importantly the vanishing density of states around the Fermi level. But as long as one is interested in processes which take place reasonably far away from the Fermi level, as is the case in the present study, we expect the effects of these shortcomings to be small. In [15, 16] internal photoemission in an otherwise bound problem had been considered. Here we are rather interested in 2PPE spectra of metal films, i.e., in external photoemission.

In what follows we extend the TD-CIS method of [15, 16] to unbound problems to allow for the laser-ejection of electrons from a metal film into the vacuum. The so-called time-energy method, known from nuclear dynamics as an efficient tool to extract information of wavepackets in asymptotic regions [18], is formulated here for many-electron dynamics in the framework of TD-CIS. For simplicity but also due to limitations in the basis set size that can be handled at present, we restrict ourselves to a one-dimensional (1D) system, in which $N$ electrons move in the positive jellium background charge density.

The 1D model system and the TD-CIS method are described in Sect. 2, followed by details of how we compute 2PPE spectra (Sect. 3). Results are presented in Sect. 4, and conclusions are given in Sect. 5.

## 2 Model system and basic methods

### 2.1 *Hartree–Fock ground state*

In the following, we restrict ourselves to a one-dimensional model. In this model a single coordinate $z$ is considered, which is the coordinate perpendicular to a metal film of thickness $d$ along which the electrons can move. For technical reasons we consider a free-standing film, centered at $z = 0$, and extending from $-d/2$ to $+d/2$. For the electron-nuclear Coulomb attraction the jellium model is used (see below).

In what follows, we will use the TD-CIS method in which the electronic wavefunction is expanded in the basis of the field-free Hartree–Fock ground state, and singly excited determinants derived thereof. The $N$-electron ground state Slater determinant, $|\Psi_0\rangle$, is determined within the closed-shell restricted HF (RHF) scheme as

$$|\Psi_0\rangle = |(\psi_1\alpha), (\psi_1\beta), \ldots, (\psi_{N/2}\alpha), (\psi_{N/2}\beta)\rangle\,, \tag{1}$$

i.e., the molecular orbitals (MOs) $\psi_\nu$ ($\nu = 1, 2, \ldots, N/2$) are occupied with two electrons of opposite ($\alpha$ and $\beta$) spin each. The MOs, and corresponding orbital energies $\varepsilon_\nu$, are determined from the spin- and field-free RHF equations as (we use atomic units throughout)

$$\left[-\frac{1}{2}\frac{\mathrm{d}^2}{\mathrm{d}z^2} + v(z) + v_\mathrm{H}(z) + \hat{v}_x\right]|\psi_\nu\rangle = \hat{f}|\psi_\nu\rangle = \varepsilon_\nu|\psi_\nu\rangle\,. \tag{2}$$

By introducing a basis set, (2) is transformed into the Roothaan–Hall matrix equations [19]. In the grid basis we use below, the basis functions are orthogonal and the Roothaan–Hall equations read

$$\underline{\underline{F}}\,\underline{C}_\nu = \varepsilon_\nu\,\underline{C}_\nu\,. \tag{3}$$

By solving (3) one obtains the $N/2$ occupied orbitals, plus $L - N/2$ unoccupied (virtual) ones, where $L$ is the size of the grid basis. The terms appearing in the Fock operator $\hat{f}$ in (2) are the kinetic energy, the external potential $v(z)$ accounting for the electron-nuclear attraction (i.e., the attraction of electrons by the background charge density $\varrho^+$ in the jellium model), as well as the Hartree potential $v_\mathrm{H}(z)$ and the exchange part, $\hat{v}_x$. In a 1D model, all electron-electron and electron-nuclear interaction terms require a regularizing parameter [20], $c$, such that

$$v(z) = -\int \frac{\varrho^+(z')}{\sqrt{(z-z')^2 + c}}\,\mathrm{d}z'$$

$$\langle\psi_\nu|v_\mathrm{H}(z)|\psi_\nu\rangle = 2\sum_{j=1}^{N/2}\iint \mathrm{d}z\,\mathrm{d}z'\frac{|\psi_j(z')|^2|\psi_\nu(z)|^2}{\sqrt{(z-z')^2+c}}$$

$$\langle\psi_\nu|\hat{v}_x(z)|\psi_\nu\rangle = -\sum_{j=1}^{N/2}\iint \mathrm{d}z\,\mathrm{d}z'\frac{\psi_j{*}(z')\psi_\nu{*}(z)\psi_j(z)\psi_\nu(z')}{\sqrt{(z-z')^2+c}}.$$

The background charge density is given, in the jellium film model, as

$$\varrho^+(z) = \begin{cases}\varrho_0^+\,, & |z| \le \frac{d}{2}\\ 0\,, & \text{else}\end{cases}\,. \tag{4}$$

For the jellium density within the film, $\varrho_0^+$, we set $\varrho_0^+ = 0.1\ e/a_0$ in the following. The parameter $c$ has no strict physical meaning and is sometimes used for adjusting computed quantities, such as the workfunction, to measured values. Here we set $c = 1.0\,a_0^2$. With this choice we obtain workfunctions in the order of a few eV.

The numerical solution of (3) is achieved by the self-consistent-field (SCF) scheme. As a basis set, a grid is employed and the Fourier grid method applied for the kinetic energy term [21–23]. The grid basis consists of $L = 1024$ grid points, hence every MO $\psi_\nu$ is represented by an $L$-component vector $\underline{C}_\nu$. The application of the ordinary Fourier grid method requires an equidistant grid, i.e., a constant grid spacing $\Delta z$. On the other hand, there are two distinct subsystems in our problem, namely (i) the metal film, and (ii) the vacuum region outside the film with very different computational needs. Namely, in the vacuum region the highest momentum of the wave function $p_\mathrm{max} = \frac{\pi}{\Delta z}$ that needs to be accounted for is typically much lower than within the film.

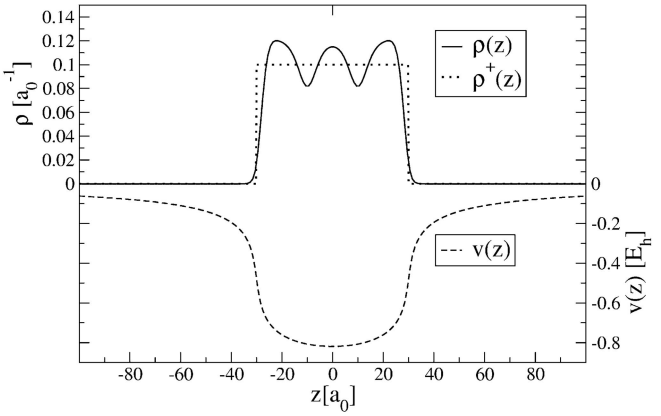


**FIGURE 1** Results of a RHF calculation for $N = 6$ electrons. Shown is the background charge density $\varrho^+(z)$, the resulting electron density $\varrho(z)$, and the external potential $v(z)$

To also cover large parts of the vacuum region and at the same time avoiding prohibitively large grids, we use the so-called mapped Fourier grid method [24]. Here a "physical grid" (with variable grid spacing along $z$) is generated from an equidistant, "mathematical grid" along a coordinate $x$, in which the Fourier transform can be performed. With a well defined mapping function $z = f(x)$, similar to that used in [10], we transform the mathematical grid to the physical grid with grid spacings $\Delta z = 1.5a_0$ within the metal film, and $\Delta z = 5.0a_0$ in the vacuum region. With $L = 1024$ we therefore can cover an area of about $|z| = z_{\max} \approx 2400a_0$, which is large enough to avoid reflection of the wavepacket from the grid boundaries for all cases to be studied below. The film thickness depends on the number of electrons, $N$ ($d = \frac{e}{\varrho_0^+} N$), and ranges from $d = 60a_0$ for $N = 6$, to $d = 200a_0$ for $N = 20$ electrons, respectively. The grid allows for electrons up to kinetic energies of $E = 0.197E_\mathrm{h}$ to be detected, which is well above what is needed below.

To illustrate the results of a field-free RHF calculation, we show in Fig. 1 for the case $N = 6$ (i) the background density $\varrho^+(z)$, (ii) the external potential $v(z)$, and (iii) the calculated electron density $\varrho(z) = \sum_{\nu=1}^{3} 2|\psi_\nu(z)|^2$. Note the three "pumps" in the electron density, reflecting the nodal structure of the occupied molecular orbitals. The three occupied orbitals have energies $\varepsilon_1 = -0.28256E_\mathrm{h} (\approx -7.7\,\mathrm{eV})$, $\varepsilon_2 = -0.26814E_\mathrm{h} (\approx -7.3\,\mathrm{eV})$, and $\varepsilon_3 = -0.24557E_\mathrm{h} (\approx -6.7\,\mathrm{eV})$, respectively, with the energy-zero taken at the vacuum level. Similar calculations have been carried out for $N = 14$ and $N = 20$. For $N = 14$ the occupied orbital space extends from $-0.29004E_\mathrm{h} (\approx -7.9\,\mathrm{eV})$ to $-0.23922E_\mathrm{h} (\approx -6.5\,\mathrm{eV})$, for $N = 20$ from $-0.29155E_\mathrm{h} (\approx -7.9\,\mathrm{eV})$ to $-0.23757E_\mathrm{h} (\approx -6.5\,\mathrm{eV})$.

### 2.2 *The time dependent configuration interaction singles (TD-CIS) method*

We now use the HF orbitals (occupied and virtual ones) to construct singly excited Slater determinants. These are then, together with the HF ground state $\Psi_0$, used as a basis set for propagating the laser-driven electronic wavefunction forward in time. By that procedure we go beyond the one-determinant models, and at the same time we allow for electron correlation, at least in the excited state manifold. Specifically, the time independent CIS wave function is expanded in the basis of singly excited Slater determinants, $\Psi_a^r$ and $\Psi_{\bar{r}}^{\bar{a}}$, which arise from the restricted HF ground state determinant $\Psi_0$ by exciting an electron with spin $\alpha$ ($\beta$) from an occupied orbital $a$ ($\overline{a}$), to a virtual orbital $r$ ($\overline{r}$). Spin-adapted singlet configuration state functions (CSFs)[25] are then obtained from

$$\Psi_i^{\mathrm{cis}} = D_{0,i}\Psi_0 + \sum_{a=1}^{N/2}\sum_{r=N/2+1}^{M} D_{a,i}^{r}\,{}^1\Psi_a^r \tag{5}$$

$${}^1\Psi_a^r = \frac{1}{\sqrt{2}}\left(\Psi_a^r - \Psi_{\bar{a}}^{\bar{r}}\right). \tag{6}$$

Being only interested in optical transitions, we discarded the triplet manifold. To diagonalize the field free system Hamiltonian $\hat{H}_{\mathrm{cis}}^0$ on this basis, the following matrix elements are required [19]:

$$\langle\Psi_0|\hat{H}_{\mathrm{cis}}^0|{}^1\Psi_a^r\rangle = 0 \tag{7}$$

$$\langle{}^1\Psi_a^r|\hat{H}_{\mathrm{cis}}^0 - E_{\mathrm{HF}}|{}^1\Psi_b^s\rangle = (\varepsilon_r - \varepsilon_a)\delta_{rs}\delta_{ab} - \langle\psi_r\psi_b|\psi_s\psi_a\rangle + 2\langle\psi_r\psi_b|\psi_a\psi_s\rangle\,. \tag{8}$$

The excited states and the excitation energies $E_i$ are determined from the matrix equation

$$\underline{\underline{H}}_{\mathrm{cis}}^0\,\underline{D}_i = E_i\underline{D}_i\,. \tag{9}$$

For the active space to construct the single excitations, (virtual) orbitals with energies up to $\varepsilon_r \le 0.15\,E_\mathrm{h}$ are included. That this choice is adequate has been checked by the proper reconstruction of the outgoing wave packet in position space. As a result of this cutoff criterion, in addition to the occupied orbitals 861, 827 and 802 virtual orbitals have been included for the $N = 6$, $N = 14$ and $N = 20$ electron cases, respectively. This leads to 2584, 5790 and 8021 CSFs (including the HF determinant).

The laser-driven electron dynamics is treated by using the $\Psi_i^{\mathrm{cis}}$ basis, and adopting the semiclassical dipole approximation for the laser-electron interaction. Specifically, we solve a time dependent Schrödinger equation

$$\mathrm{i}\dot{\Psi}^{\mathrm{cis}}(t) = \hat{H}_{\mathrm{cis}}(t)\,\Psi^{\mathrm{cis}}(t) \tag{10}$$

with

$$\hat{H}_{\mathrm{cis}}(t) = \hat{H}_{\mathrm{cis}}^0 - \hat{\mu}F(t)\,. \tag{11}$$

Here, $\hat{\mu} = -\sum_{i=1}^{N} ez_i$ is the dipole operator, and $F(t)$ the electric field of the two laser pulses with a time delay $\Delta t = t_2 - t_1$:

$$F(t) = f_1(t)\cos[\omega(t - t_1)] + f_2(t)\cos[\omega(t - t_2)]\,. \tag{12}$$

In (12) we have assumed that both lasers have the same frequency, $\omega$. For the field envelopes

$$f_i(t) = \begin{cases} f_{\max}\cos^2\left[\frac{\pi}{2\sigma}(t - t_i)\right], & t_i - \sigma < t < t_i + \sigma \\ 0\,, & \text{else} \end{cases} \quad ; i = 1, 2 \tag{13}$$

we assume a $\cos^2$ form, and the same maximal field strength $f_{\max}$ and pulse width $\sigma$. In the following, we take $\hbar\omega = 0.155 E_\mathrm{h}$ ($\approx 4.2$ eV), $\sigma = 826.8\hbar/E_\mathrm{h}$ ($= 20$ fs), $f_{\max} = 0.001 E_\mathrm{h}/(ea_0)$ ($\approx 5.1 \times 10^8$ V/m), and the delay time $\Delta t$ is varied between 0 and about $4500\hbar/E_h$ ($\approx 100$ fs). Since the time dependent CIS wave function is expanded in the basis of $K$ time independent CIS eigenfunctions $\Psi_i^{\mathrm{cis}}$, the expansion coefficients become time dependent, i.e.,

$$\Psi^{\mathrm{cis}}(t) = \sum_i^K D_i(t)\Psi_i^{\mathrm{cis}}\,, \tag{14}$$

with the initial condition

$$\Psi^{\mathrm{cis}}(t_0) = \Psi^{\mathrm{cis}}(t=0) = \Psi_0\,. \tag{15}$$

The numerical propagation of the electronic wavefunction is done as follows. As long as the field is on, a split operator technique [26] is used:

$$|\Psi(t+\Delta\tau)\rangle = \mathrm{e}^{\frac{-i\hat{H}_0\Delta\tau}{2}}\hat{U}^\dagger \mathrm{e}^{iF(t)\hat{\tilde{\mu}}\Delta\tau}\hat{U}\mathrm{e}^{\frac{-i\hat{H}_0\Delta\tau}{2}}|\Psi(t)\rangle\,. \tag{16}$$

Here, $\hat{\tilde{\mu}}$ is the diagonal dipole operator in its eigenfunction space and $\hat{U}$ transforms the eigenfunctions of $\hat{H}^0_{\mathrm{cis}}$ to those of $\hat{\mu}$. The propagation time step used is $\Delta\tau = 1.0\,\hbar/E_\mathrm{h}$, which gave converged results. When the laser is off, the time propagation is given analytically as

$$|\Psi(t+\Delta\tau)\rangle = \mathrm{e}^{-i\hat{H}_0\Delta\tau}|\Psi(t)\rangle\,. \tag{17}$$

## 3 Simulation of 2PPE spectra

Due to the interaction of the electrons with the laser field photoelectrons can be ejected into the vacuum. The laser parameters are such that the first pulse will not deliver enough energy to do so, but the second one may excite electrons to above $E = 0$ (see below). As an example, we show in Fig. 2 the electron density $\varrho(z,t)$ for the six-electron system, for a delay time $\Delta t = 0$ (fully overlapping pulses). Both pulses start at $t = 0$ and are maximal at $t_1 = 826.8\hbar/E_h$. We note that some portion of the electron density is being ejected from the metal film. Due to our symmetric, free-standing film model simultaneous electron arrays in positive and negative $z$ directions are seen. Our aim is to analyze the photoionization signal, $P$, as a function of (kinetic) energy $E$, of the emitted electron, and delay time, i.e., $P(E, \Delta t)$. To determine the kinetic energy of the electron one would have to represent $\Psi(t)$ on a grid, which must in addition be large enough to avoid reflection of the wavepacket from the grid boundaries. Such a direct approach is virtually impossible as for an $L$-point grid and $N$-electron system, the wavefunction is a vector of size $L^N$. For this reason we use a new method that is based on the time-energy method of nuclear dynamics [27], for analyzing the outgoing electron wave packet in asymptotic regions of the potential.

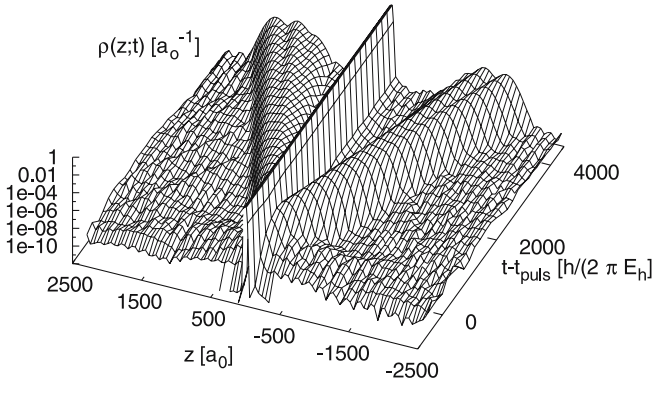


**FIGURE 2** Time dependent electron density $\varrho(z,t)$, for $N = 6$ and $\Delta t = 0$. See text for further details

### 3.1 *Time-energy method*

The time-energy method has been used originally for computing partial cross sections in molecular photodissociation [18, 27–29]. Balint–Kurti et al. [18] have shown that this time dependent formulation is formally equivalent to the well studied time independent formulation [30, 31]. The basic idea behind this method is to calculate the projection coefficients of the outgoing wave packet onto asymptotic fragment states and use a time-energy Fourier transform to get these projection coefficients at all energies which are adequately represented by the initial wave packet [32].

When applied to our problem, we have to choose a sufficiently large value $R$ of the electron coordinate such that $\frac{\mathrm{d}v(z)}{\mathrm{d}z}|_{(z=R)} \approx 0$. As soon as the wave packet passes through $R$, it is analyzed with the help of fragment wave functions, the so-called exit channels, $\phi_j$. The total reaction (ionization) probability is obtained by recording the time dependent projection coefficients $C_j(R,t)$, which arise from projection of the $N$-particle wave function $\Psi^{\mathrm{cis}}(z_1 = R, z_2, \ldots, z_N, \omega_1, \omega_2, \ldots, \omega_N, t)$ onto fragment states $\phi_j(z_2, \ldots, z_N, \omega_2, \ldots, \omega_N)$. The $\phi_j$ describe the $N-1$ electrons which are excepted form the reaction. Hence:

$$C_j(R,t) = N\int \Psi^{\mathrm{cis}}(z_1 = R, z_2, \ldots, z_N, \omega_1, \omega_2, \ldots, \omega_N, t) \times \phi_j(z_2, \ldots, z_N, \omega_2, \ldots, \omega_N)\,\mathrm{d}z_2 \ldots \mathrm{d}z_N\,\mathrm{d}\omega_2 \ldots \mathrm{d}\omega_N. \tag{18}$$

The factor $N$ accounts for the $N$ indistinguishable electrons. The $\omega_j$ denote the spin coordinates. The projections are carried out until the propagating wave packet has passed the projection point. After projection the wave packet is no longer needed and can be absorbed by an optical potential, for example. (For up to $N = 20$ electrons and the grid size adopted here, no absorbers were needed but may become necessary when more electrons are to be considered.) In practice we use $R = 750\,a_0$ for $N = 6$, and $R = 500\,a_0$ for $N = 14$ and $N = 20$. A time-energy Fourier transform then yields the energy dependent projection coefficients:

$$C_j(R,E) = \int_{-\infty}^{\infty} C_j(R,t)\mathrm{e}^{iEt}\,\mathrm{d}t\,. \tag{19}$$

The total, energy-resolved reaction probability, i.e., the 2PPE signal, is obtained from

$$P(E) = \sum_j |C_j(R, E)|^2 \,. \tag{20}$$

### 3.2 *Specification of the exit channels*

The integration in (18) cannot be done straightforwardly, because the integration in (18) and the summation in (20) do not commute. So one would have to do both the integration in (18) and the reconstruction of $\Psi^{\text{cis}}$ in position space for every $j$ – thus the $L^N$ storage problem prevails. (For $N = 20$ and $L = 1024$, $\approx 1.6 \times 10^{60}$ numbers would have to be stored). To avoid this, the integration in (18) is done analytically by using a suitable analytical ansatz for the exit channels. The most obvious choice to describe a system consisting of $N-1$ electrons is a restricted Slater determinant of the type:

$$\phi_j(z_2, \ldots, z_N, \omega_2, \ldots, \omega_N) = \frac{1}{(N-1)!} \times \sum_{\mathcal{P}} (-1)^{\chi(\mathcal{P})} \chi^j_{p_1}(z_2, \omega_2) \chi^j_{p_2}(z_3, \omega_3) \ldots \chi^j_{p_{N-1}}(z_N, \omega_N) \,. \tag{21}$$

Here, $\chi^j_p(z, \omega)$ are spin orbitals (spatial orbital $\times$ spin function), and the sum runs over all $(N-1)!$ permutations. The specific choices of the $\phi_j$ will be given below.

It has to be mentioned that, as one problem, the exit channels $\phi_j$ are not exact eigenfunctions of the reduced ($z_1 \to \infty$) Hamiltonian of the system:

$$\hat{H}_{\text{red}}(z_2, z_3, \ldots, z_N, \omega_1, \omega_2, \omega_3, \ldots, \omega_N; z_1 \to \infty)\phi_j \neq \varepsilon_j \phi_j \tag{22}$$

The energies $\varepsilon_j$, however, are needed to determine the kinetic energy of the emitted electrons. Here we approximate the energies $\varepsilon_j$ of the exit channels by using Koopmans' theorem [19], i.e., by energy differences of orbital energies (see below). We also mention that exact exit channels $\Phi_n$ can be defined by diagonalizing the matrix $\underline{\underline{H}}_{\text{red}}$, expressed in the basis of the $\phi_j$:

$$(\hat{H}_{\text{red}})_{jj'} = \langle \phi_j | \hat{H}_{\text{red}} | \phi_{j'} \rangle \Longrightarrow \Phi_n = \sum_i A^n_i \phi_i \,. \tag{23}$$

The comparison of the results obtained by Koopmans' theorem with the exact results will be done in future work.

### 3.3 *Formalism*

Using the Slater–Condon rules and combinatorial considerations to evaluate (18), one finds that only three different kinds of Slater determinants, which we denote here as $\phi^I_j$, $\phi^{II}_j$, and $\phi^{III}_j$, have non-vanishing contributions to the ionization probability. With $j = 2n-1$ for odd $j$ and $j = 2n$ for even $j$, these Slater determinants are:

$$\begin{aligned} &\phi^I_{2n} = \Psi_0 \setminus \{\psi^\alpha_n\} \\ &\phi^I_{2n-1} = \Psi_0 \setminus \{\psi^\beta_n\} \\ &n = 1, \ldots, A = s_1 \end{aligned} \tag{24a}$$

$$\begin{aligned} &\phi^{II}_{2n} = \Psi^{\bar{r}}_{\bar{a}} \setminus \{\psi^\alpha_k\} \\ &\phi^{II}_{2n-1} = \Psi^r_a \setminus \{\psi^\beta_k\} \\ &n = 1, \ldots, A^2 B = s_2 \end{aligned} \tag{24b}$$

$$\begin{aligned} &\phi^{III}_{2n} = \Psi^r_a \setminus \{\psi^\alpha_k\} \\ &\phi^{III}_{2n-1} = \Psi^{\bar{r}}_{\bar{a}} \setminus \{\psi^\beta_k\} \\ &n = 1, \ldots, \tfrac{A(A-1)B}{2} = s_3 \,. \end{aligned} \tag{24c}$$

Examples are shown in Fig. 3. Here, $A = N/2$ and $B$ are the numbers of previously occupied and virtual (unoccupied) MOs, respectively. Note that the index $k$ enumerates an occupied orbital of the HF ground state Slater determinant and it is $k \neq a$. A few words of explanation. Case I (24a), Fig. 3a: Here, $N-1$ electrons remain in previously occupied molecular orbitals. We distinguish between even and odd exit wave functions. The even (odd) exit channels have lost an $\alpha$ ($\beta$) electron, i.e., the ejected electron at $z_1 = R$ has $\alpha$ ($\beta$) spin. There are $2A = N$ different exit channels of this type. It can easily be seen from (18) that all $N$-particle functions $\Psi^{\text{cis}}_i$ contribute to $P(E)$, which have the reactive (ejected) electron in a former virtual orbital. Cases II and III 24(b,c); Fig. 3b,c: These exit channels have one electron in a previously virtual orbital, while $N-2$ electrons are in the previously occupied orbitals. This time the electron associated with the reactive coordinate is ejected from a previously occupied orbital. In both cases the number of channels is proportional to the number of former virtual orbitals $B$ which were included in the active CIS space.

The total ionization probability at energy $E$, i.e., the 2PPE signal, is given by

$$P(E) = 2\left\{ \sum_{n=1}^{s_1} |C^I_{2n}(R, E)|^2 + \sum_{n=1}^{s_2} |C^{II}_{2n}(R, E)|^2 + \sum_{n=1}^{s_3} |C^{III}_{2n}(R, E)|^2 \right\} \tag{25}$$

with

$$\begin{aligned} |C^I_{2n}(R, E)\rangle &= \sqrt{N} \int \left( \frac{1}{\sqrt{2}} \sum_{r \in \mathcal{V}} \mathcal{C}^r_n(t)\psi_r(R) + \mathcal{C}_0(t)\psi_n(R) \right) |\alpha\rangle e^{iEt}\, dt \\ |C^{II}_{2n}(R, E)\rangle &= -\sqrt{\frac{N}{2}} \int \mathcal{C}^r_a(t)\psi_k(R)|\alpha\rangle e^{iEt}\, dt \\ |C^{III}_{2n}(R, E)\rangle &= \sqrt{\frac{N}{2}} \int \left( \mathcal{C}^r_a(t)\psi_k(R) + \mathcal{C}^r_k(t)\psi_a(R) \right) |\alpha\rangle e^{iEt}\, dt. \end{aligned} \tag{26}$$

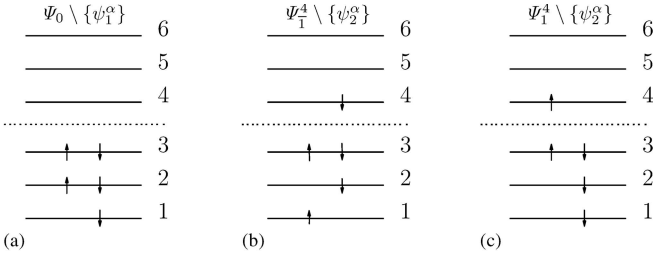


**FIGURE 3** Examples of the different types of exit channels defined in (24), represented within a restricted orbital scheme ($A = B = 3$)

The $\mathcal{C}_x^y(t)$ are given as (see (5) and (14)):

$$\mathcal{C}_x^y(t) = \sum_{i=1}^{K} D_i(t)\, D_{x,i}^y \,, \tag{27}$$

where $\mathcal{V}$ denotes the space of virtual orbitals. The proof of (25) is outlined in the Appendix.

## 4 Results

The calculations of 2PPE spectra were done for 1D model systems with 6, 14 and 20 electrons, respectively. As outlined before, the energies of the highest occupied molecular orbitals range from $-0.24557\,E_\mathrm{h}$ (for $N = 6$) to $-0.23757\,E_\mathrm{h}$ (for $N = 20$). With the mentioned laser pulse energies of $\hbar\omega = 0.155\ E_\mathrm{h}$ for both pulses, we therefore expect – in a simple independent electron model – kinetic energies up to $0.064 E_\mathrm{h} (\approx 1.8\,\mathrm{eV})$ for $N = 6$, and $0.072 E_\mathrm{h} (\approx 2.0\,\mathrm{eV})$ for the emitted electrons. For a more exact analysis, the time-energy method as outlined above is applied, with the analysis done at every $20\,\hbar/E_\mathrm{h}$.

### 4.1 *Time-resolved 2PPE spectra:* $\Delta t = 0$

The energy-resolved 2PPE spectra, $P(E)$, are shown for $N = 6$ to $N = 20$ for zero delay ($\Delta t = t_2 - t_1 = 0$) in Fig. 4. Considering Fig. 4a we find, for $N = 6$, a signal with three maxima, which reflect roughly the position of the previously occupied molecular orbitals. More quantitatively, $\varepsilon_i + 2\hbar\omega$ is $0.027 E_\mathrm{h}$, $0.042 E_\mathrm{h}$, and $0.064 E_\mathrm{h}$, respectively, in good agreement with the values $0.028 E_\mathrm{h}$, $0.042 E_\mathrm{h}$, and $0.063 E_\mathrm{h}$ of Fig. 4a.

It is also found that the peaks of the signals in Fig. 4 have a certain finite width, due to the spectral width of the exciting laser, but also intermediate and final state effects.

The fact that the 2PPE spectrum does not show, however, any clear signature of previously unoccupied (intermediate) states is due to the fact that in our 1D jellium model, the density of states in the "active energy range" is high and structureless, in contrast to 2PPE spectroscopy of image potential states at metals with a projected band gap [3]. In general, therefore, the 2PPE signal is determined by initial, intermediate, and final state effects, as well as by the laser pulses.

In Fig. 4b we demonstrate, for $N = 6$, that only channels of type I, i.e., $\phi_j^I$, contribute significantly to the 2PPE signal.

In contrast, types II and III contribute almost nothing. This is understandable from (26), where previously occupied orbitals $\psi_k$ for case II and $\psi_k$ and $\psi_a$ for case III, at the point of analysis, $R$, enter. Since $\psi_a(R)$ and $\psi_k(R)$ are vanishingly small for large $R$, these orbitals cannot contribute much to the 2PPE signal.

In passing we note that a measure for the accuracy of the computed 2PPE signal is given by the residual ionization probability for $E \le 0$, also shown in Fig. 4b. This residual probability is very small, showing that the size of the grid and the cutoff for virtual orbitals have been chosen carefully.

Similarly, for $N = 14$ and $N = 20$ we expect seven and ten peaks, respectively. In Fig. 4c and d, however, not all of these peaks can be resolved because of the finite width of the main peaks. It is possible, on the other hand, to define orbital-resolved ionization probabilities from (25). Namely, neglecting the contributions of channels II and III, the 2PPE signal of (25) reads

$$P(E) \approx 2 \sum_{n=1}^{s_1} |C_{2n}^I(R, E)|^2 = \sum_{\nu=1}^{N/2} P_\nu(E) \,, \tag{28}$$

where $P_\nu(E)$ is the orbital-resolved 2PPE signal, measuring contributions from occupied molecular orbital $\psi_\nu$. When plot-

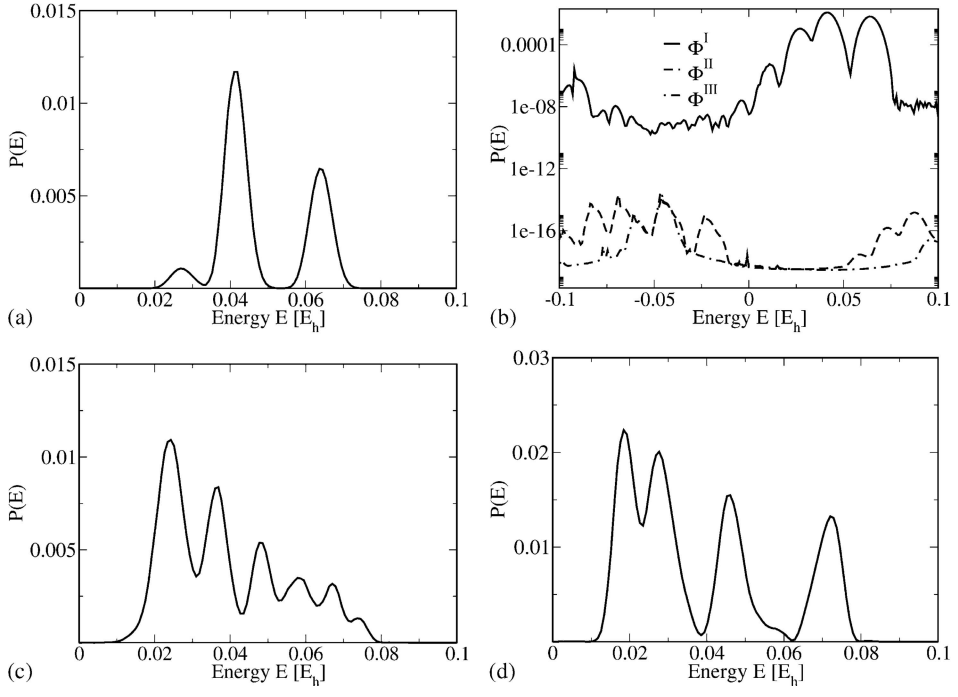


**FIGURE 4** Energy-resolved 2PPE spectra for $\Delta t = 0$ and $N = 6$ (**a**), 14 (**c**) and 20 electrons (**d**), respectively. Comparison of the contribution of exit channels of type I, II and III, for $N = 6$ (**b**)

ting the $P_\nu(E)$ separately, one can therefore decompose the total signal into orbital-resolved ones, i.e., seven peaks for $N = 14$, and ten peaks for $N = 20$.

### 4.2 *Time-resolved 2PPE spectra:* $\Delta t \neq 0$

In a further step TR-2PPE spectra $P(E, \Delta t)$ were calculated for non-zero delay times. Specifically, we consider the $N = 6$ electron case, and the three (kinetic) energies where the energy-resolved 2PPE signal for $\Delta t = 0$ is maximal (cf. Fig. 4a). The TR-2PPE spectra for the three selected energies are shown in Fig. 5a–c. By the first pulse, we excite electrons from previously occupied orbitals to previously empty ones below the vacuum level. Due to electron-electron scattering, the prepared intermediate state "looses memory". In an effective one-electron picture one would assign a certain lifetime, $\tau$, to the intermediate state. The second pulse then not necessarily finds the excited electron where it used to be, hence it cannot be ejected, and at longer delay times $\Delta t$ we expect that the 2PPE signal goes down. From the speed of the decay of the signal, the relaxation time of the excited electrons can estimated.

In Fig. 5 we see indeed a rapid decay of the 2PPE signal with delay time, $\Delta t$. We note that the overall signal decays within about $800\hbar/E_\mathrm{h} (\approx 20\,\mathrm{fs})$ to about half of its original value. However, as this is also the order of magnitude for the cross correlation width of the two laser pulses, a more accurate "lifetime" of the intermediate states cannot be deduced here. For larger energies $E$, electrons are excited into intermediate states which are higher above the Fermi energy. For these, a shorter lifetime is expected – in a 3D Fermi liquid model [33, 34] according to $\tau_n \propto (E_n - E_F)^{-2}$, when $E_n$ is the energy of the intermediate state. In real systems, but notably also in lower-dimensional models, the scaling is weaker. In fact in Fig. 5 we find only a weak energy-dependence of the initial falloff time.

The analysis is hampered by the fact that in our model a clear falloff is hard to determine due to (i) a rapidly oscillating fine structure, and (ii) partial recurrences of the signal. (iii) Finally, by using lasers of finite widths a set of intermediate states is excited, each with an individual "lifetime". The fine structure is due to the fact that the two laser pulses interfere constructively and destructively, depending on the delay time, hence the 2PPE signal oscillates with the laser frequency $\hbar\omega$ between small and large signals. This effect can also be seen, e.g., in two-pulse correlation experiments on laser-driven electron transport through MIM contacts [16]. The recurrences, on the other hand, are probably due to our limited 1D model, and the few electrons considered.

In a one electron picture one would say that the electron initially in the active energy space can only decay by internal energy redistribution to other electrons, but sooner or later it will reenter the active energy space, due to the closed quantum system model.

In a 3D model with more electrons, the phase space volume into which electrons can scatter is much bigger, hence recurrence times are expected to be much longer than the time span covered by Fig. 5. In summary, the decay of the TR-2PPE is non-exponential, and care must be taken when evaluating "lifetimes".

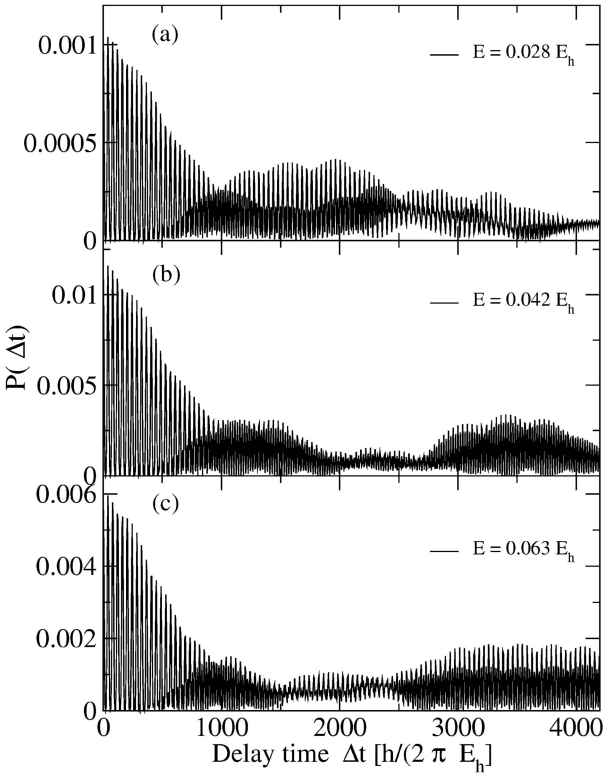


**FIGURE 5** TR-2PPE spectra for the 6-electron system, at three selected energies

## 5 Conclusions and outlook

We have computed correlation-corrected excited states of electrons confined in a metal film by using the configuration interaction singles (CIS) formalism. The calculations were carried out within a 1D jellium model. By extending the method to an explicitly time dependent form (TD-CIS), the electron-field interaction could explicitly be accounted for. A new method has been devised for analyzing the outgoing electronic wave packet. Orbital-resolved 2PPE signals were introduced. Both energy- and time-resolved 2PPE spectra were computed. The latter allows one to deduce "lifetimes" of electronically excited states due to electron-electron scattering, despite, as shown, such an assignment is not straightforward and needs further attention in the future.

In future work, we will extend the present model to include more electrons, thus shifting the recurrence times to longer periods. An extension to 3D will be difficult for nanostructured materials, but should be possible for smaller systems. The introduction of electron-phonon coupling is another difficult task, but fortunately not needed for short-time dynamics. Within the reduced-dimensionality models, one may still introduce band structure effects by going beyond the simple jellium model. By this procedure one will be able to detect not only bulk states, but also surface states (including image potential states) and adsorbate states, for example, as intermediate states.

**ACKNOWLEDGEMENTS** We thank Peter Saalfrank for fruitful discussions and gratefully acknowledge support of this work by the Deutsche Forschungsgemeinschaft through project Sa 547/5 (SPP-1093).

## Appendix: A proof of (25)

Starting from (18) for the time dependent projection coefficients $C_j(R,t)$

$$
\begin{aligned}
&C_j(R,t) = \\
&N\int \Psi^{\mathrm{cis}}(R,z_2,\ldots,z_N,\omega_1,\omega_2,\ldots,\omega_N,t) \\
&\qquad\times\phi_j(z_2,\ldots,z_N,\omega_2,\ldots,\omega_N)\,\mathrm{d}z_2\ldots\mathrm{d}z_N\,\mathrm{d}\omega_2\ldots\mathrm{d}\omega_N
\end{aligned}
$$

we get by inserting (5),(14)

$$
\begin{aligned}
&\Longrightarrow C_j(R,t) = N \\
&\times\int\sum_{i=1}^{K} D_i(t)\Psi_i^{\mathrm{cis}}\phi_j(z_2,\ldots,\omega_N)\,\mathrm{d}z_2\ldots\mathrm{d}\omega_N \\
&= N\sum_{i=1}^{K}\int D_i(t)\left(\sum_{S_{ar}} D^r_{a,i}{}^1|\Psi^r_a\rangle + D_{0,i}\Psi_0\right)\phi_j\,\mathrm{d}z_2\ldots\mathrm{d}\omega_N \\
&= \frac{N}{\sqrt{2}}\sum_{i=1}^{K}\sum_{S_{ar}}\int D_i(t)D^r_{a,i}(\Psi^r_a-\Psi^{\bar{r}}_{\bar{a}})\phi_j\,\mathrm{d}z_2\ldots\mathrm{d}\omega_N \\
&\quad + N\sum_{i=1}^{K}\int D_i(t)D_{0,i}\Psi_0\phi_j\,\mathrm{d}z_2\ldots\mathrm{d}\omega_N\,. \qquad (A.1)
\end{aligned}
$$

Here $S_{ar}$ is a composite index numbering single excitations used. Furthermore,

$$
\begin{aligned}
&\sum_{i=1}^{K}\sum_{S_{ar}}\int D_i(t)D^r_{a,i}\Psi^r_a\phi_j\,\mathrm{d}z_2\ldots\mathrm{d}\omega_N \\
&= \sum_{S_{ar}}\mathcal{C}^r_a(t)\frac{1}{\sqrt{N!}} \\
&\times\sum_{\mathcal{P}}(-1)^{\chi(\mathcal{P})}\chi_{p_1}(R,\omega_1)\chi_{p_2}(z_2,\omega_2)\times\ldots\times\chi_{p_N}(z_N,\omega_N) \\
&\times\frac{1}{\sqrt{(N-1)!}}\sum_{\mathcal{Q}}(-1)^{\chi(\mathcal{Q})} \\
&\chi_{q_1}(z_2,\omega_2)\chi_{q_2}(z_3,\omega_3)\times\ldots\times\chi_{q_{(N-1)}}(z_N,\omega_N)\times\mathrm{d}z_2\ldots\mathrm{d}\omega_N \\
&= C^1_j(R,t) \qquad (A.2) \\
&\sum_{i=1}^{K}\sum_{S_{ar}}\int D_i(t)D^r_{a,i}\Psi^{\bar{r}}_{\bar{a}}\phi_j\,\mathrm{d}z_2\ldots\mathrm{d}\omega_N = C^2_j(R,t)\,.
\end{aligned}
$$

We obtain for case I:

$$
\begin{aligned}
&C^1_{2n} = \frac{1}{\sqrt{N}}\sum_{r\in\mathcal{V}}\mathcal{C}^n_r\psi_r(R)\alpha(\omega) \\
&C^1_{2n+1} = 0 \\
&C^2_{2n} = 0 \qquad (A.3) \\
&C^2_{2n+1} = \frac{1}{\sqrt{N}}\sum_{r\in\mathcal{V}}\mathcal{C}^n_r\psi_r(R)\alpha(\omega)\,.
\end{aligned}
$$

Finally we get the result:

$$
\begin{aligned}
C^I_j(R,t) &= (-1)^j\sqrt{N}\left(\frac{1}{\sqrt{2}}\sum_{r\in\mathcal{V}}\mathcal{C}^r_{\tilde{n}}(t)\psi_r(R)+\mathcal{C}_0(t)\psi_{\tilde{n}}(R)\right) \\
&\times\begin{cases}\alpha(\omega_1): & j\text{ even}\\ \beta(\omega_1): & j\text{ odd}\end{cases} \qquad (A.4)
\end{aligned}
$$

$$
\tilde{n} = \begin{cases}\frac{j}{2}: & j\text{ even}\\ \frac{j-1}{2}: & j\text{ odd}\end{cases}\,. \qquad (A.5)
$$

Analogous for case II and III:

$$
C^{II}_j(R,t) = (-1)^{j+1}\sqrt{N/2}\mathcal{C}^r_a(t)\psi_k(R)\times\begin{cases}\alpha(\omega_1): & j\text{ even}\\ \beta(\omega_1): & j\text{ odd}\end{cases}\,. \qquad (A.6)
$$

$$
\begin{aligned}
C^{III}_j(R,t) =&(-1)^j\sqrt{N/2}(\mathcal{C}^r_a(t)\psi_k(R)+\mathcal{C}^r_k(t)\psi_a(R)) \\
&\times\begin{cases}\alpha(\omega_1): & j\text{ even}\\ \beta(\omega_1): & j\text{ odd}\end{cases}\,. \qquad (A.7)
\end{aligned}
$$

Additionally

$$
\begin{aligned}
\langle C_{2n}|C_{2n}\rangle &= \int\mathrm{d}\omega\langle C_{2n}|\alpha\rangle\langle\alpha|C_{2n}\rangle \\
&= \int\mathrm{d}\omega(-1)(-1)\langle C_{2n+1}|\beta\rangle\langle\beta|C_{2n+1}\rangle \\
&= \langle C_{2n+1}C_{2n+1}\rangle\,. \qquad (A.8)
\end{aligned}
$$

Applying now (19), we obtain (25).

## REFERENCES


1 H. Guo, P. Saalfrank, T. Seideman: Prog. Surf. Sci. **62**, 239 (1999)
2 M. Wolf, M. Aeschlimann: Phys. Bl. **54**, 145 (1998)
3 U. Höfer, I.L. Shumay, C. Reuß, U. Thomann, W. Wallauer, T. Fauster: Science **277**, 1480 (1997)
4 T. Fauster, C. Reuß, I.L. Shumay, M. Weinelt: Chem. Phys. **251**, 111 (2000)
5 C.B. Harris, N.-H. Ge, R.L. Lingle, J.D. McNeill, C.M. Wong: Ann. Rev. Phys. Chem. **48**, 711 (1997)
6 H. Petek, M.J. Weida, H. Nagano, S. Ogawa: Science **288**, 1402 (2000)
7 N. Pontius, G. Lüttgens, P.S. Bechthold, M. Neeb, W. Eberhardt: J. Chem. Phys. **115**, 10479 (2001)
8 J.P. Gauyacq, A.G. Borisov, G. Raseev: Surf. Sci. **490**, 99 (2001)
9 A.G. Borisov, J.P. Gauyacq, S.V. Shabanov: Surf. Sci. **487**, 243 (2001)
10 T. Klamroth, P. Saalfrank, U. Höfer: Phys. Rev. B **64**, 035420 (2001)
11 J. Sjakste, A.G. Borisov, J.P. Gauyacq: Nucl. Instrum. Methods in: Phys. B **203**, 49 (2003)
12 W.-D. Schöne: Int. J. Mod. Phys. B **17**, 5655 (2003)
13 P.M. Echenique, R. Berndt, E.V. Chulkov, T. Fauster, A. Goldmann, U. Höfer: Surf. Sci. Rep. **52**, 219 (2004)
14 F. Calvayrac, P.-G. Reinhard, E. Suraud, C.A. Ullrich: Phys. Rep. **337**, 493 (2000)
15 T. Klamroth: Phys. Rev. B **68**, 245421 (2003)
16 A. Thon, M. Merschdorf, W. Pfeiffer, T. Klamroth, P. Saalfrank, D. Diesing: Appl. Phys. A **78**, 189 (2004)
17 J.B. Foresman, M. Head-Gordon, J.A. Pople, M.J. Frisch: J. Phys. Chem. **96**, 135 (1992)
18 G.G. Balint-Kurti, R.N. Dixon, C.C. Martson: J. Chem. Soc. Faraday Trans. **86**, 1741 (1990)

19 A. Szabo, N.S. Ostlund: *Modern Quantum Chemistry* (Dover Publications Inc., Mineola, New York 1989) 1st (revised) edn.
20 R. Grobe, J.H. Eberly: Phys. Rev. A **48**, 4664 (1993)
21 R. Kosloff: J. Phys. Chem. **92**, 2087 (1988)
22 C.C. Martson, G.G. Balint-Kurti: J. Chem. Phys. **91**, 3571 (1989)
23 D.T. Colbert, W.H. Miller: J. Chem. Phys. **96**, 1982 (1992)
24 V. Kokoouline, O. Dulieu, R. Kosloff, F. Masnou-Seeuws: J. Chem. Phys. **110**, 9865 (1999)
25 R. Paunz: *Spin Eigenfunctions* (Plenum, New York 1979)
26 A.D. Bandrauk, E. Aubanel, S. Chelkowski: In: *Femtosecond Chemistry*, ed. by J. Manz, L. Wöste (Verlag Chemie, 1995), Vol. 2, Chapt. 25, pp. 731–742
27 G.G. Balint-Kurti, R.N. Dixon, C.C. Martson, A. Mulholland: Comp. Phys. Commun. **63**, 126 (1991)
28 N. Balakrishnan, N. Sathyamurthy: Chem. Phys. Lett. **240**, 119 (1995)
29 D. Neuhauser, M. Baer, R.S. Judson, D.J. Kouri: Comp. Phys. Commun. **63**, 460 (1991)
30 G.G. Balint-Kurti, M. Shapiro: Chem. Phys. **61**, 137 (1981)
31 M. Shapiro, R. Bersohn: Annu. Rev. Phys. Chem. **33**, 409 (1982)
32 N. Balakrishnan, C. Kalyanaraman, N. Sathyamurthy: Phys. Rep. **280**, 79 (1997)
33 J.J. Quinn, R.A. Ferrell: Phys. Rev. **112**, 812 (1958)
34 J.J. Quinn: Phys. Rev. **126**, 1453 (1962)